# Inactivation Effects of Non-Thermal Atmospheric-Pressure Helium Plasma Jet on *Staphylococcus aureus* Biofilms

Zimu Xu, Jie Shen, Zelong Zhang, Jie Ma, Ronghua Ma, Ying Zhao, Qiang Sun, Shulou Qian, Hao Zhang, Lili Ding,* Cheng Cheng,* Paul K. Chu,* Weidong Xia

The antimicrobial effects and mechanism of helium atmospheric-pressure plasma jet (APPJ) treatment on *Staphylococcus aureus* biofilms are evaluated *in vitro*. The *S. aureus* biofilms are more resistant to the plasma treatment than adherent bacteria. The APPJ-treated *S. aureus* biofilms disclose a depth/layer-related intra-bacterial ROS accumulation effect. Plasma exposure may induce bacterial oxidative stress and trigger the production of intracellular reactive oxygen species (ROS) in the biofilms, which possibly contributes to bacteria death in addition to direct etching from the exterior of bacteria. The findings provide insights into the mechanism of biofilm inactivation by plasma reactive species and plasma-induced intracellular ROS.

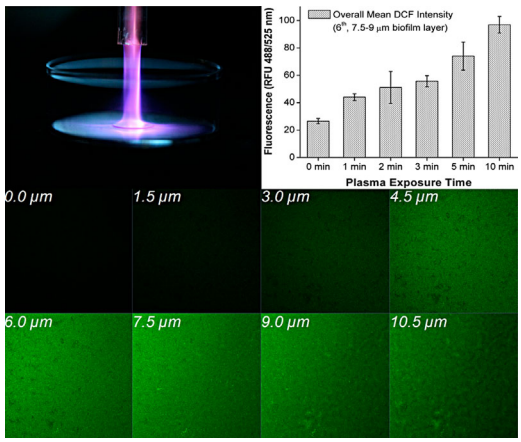


## 1. Introduction

A microbial biofilm constitutes a dynamic environment in which bacteria attach to each other and are embedded in self-produced extracellular polymeric substances (EPS) consisting of polysaccharides, water, and excreted cellular products including lysed cell debris and macromolecules creating a colonizing structure on living or inert surfaces. Biofilms can be initiated by planktonic bacteria and are responsible for undesirable effects resulting in chronic wounds and nosocomial as well as device- and implant-associated infections. Physiologically, bacteria in biofilms usually have significantly different properties from planktonic or adherent ones of the same species due to the dense and protective EPS as well as regulatory mechanism of cell-to-cell quorum sensing (QS) allowing the biofilm bacteria to coordinate with each other *via* a specific communication and conjugation system to counteract environmental stress synergistically.[1–3] Biofilms possess increased resistance to the host immune defense and antibiotics and the antibiotic

Z. Xu, Z. Zhang, Q. Sun, S. Qian, W. Xia
Department of Thermal Science and Energy Engineering, University of Science and Technology of China, Hefei, Anhui Province 230026, P. R. China
Z. Xu, R. Ma, H. Zhang, L. Ding, W. Xia
School of Life Science, University of Science and Technology of China, Hefei, Anhui Province 230026, P. R. China
E-mail: llding@ustc.edu.cn
J. Shen, Y. Zhao, C. Cheng
Institute of Plasma Physics, Chinese Academy of Sciences, P. O. Box 1126, Hefei 230031, P. R. China
J. Ma, C. Cheng, W. Xia
Center of Medical Physics and Technology, Hefei Institutes of Physical Science, Chinese Academy of Sciences, Hefei 230031, P. R. China
C. Cheng, P. K. Chu
Department of Physics and Materials Science, City University of Hong Kong, Tat Chee Avenue, Kowloon, Hong Kong, P. R. China
E-mail: chengcheng@ipp.ac.cn, paul.chu@cityu.edu.hk

*Plasma Process. Polym.* **2015,** DOI: 10.1002/ppap.201500006

resistance can increase by a thousand times in some instances.[4] Therefore, biofilm-associated diseases often lead to high morbidity, mortality, and high healthcare costs.[5] It is challenging to fight biofilm-associated diseases because conventional methods to control microbial growth tend to be inefficient and it is therefore imperative to develop more effective methods to inactivate biofilm bacteria on human tissues, biomaterials, and medical devices.

Plasma medicine, an emerging and developing interdisciplinary research field encompassing plasma science, physics, biology, and medicine, provides novel therapeutic strategies and methods to cure biofilm-associated diseases or chronic wounds.[6,7] Atmospheric-pressure plasmas, especially atmospheric-pressure plasma jets (APPJs), are typically operated at near room temperature thus rendering them suitable for direct application to heat-sensitive substrates and human tissues.[8–17] The transient nature and associated thermal non-equilibrium of APPJs lead to enhanced plasma chemistry as well as fast and effective transport of charged species to the targets.[18,19] APPJs contain a mixture of charged particles and chemically active species emitting ultra-violet (UV) radiation and it is believed that the reactive species generated from the plasmas (e.g., $O_3$, $O_2^-$, NO, $H_2O_2$, O, and OH) contribute to the anti-microbial effects by inducing damage of lipids, proteins, DNA, etc., leading to cellular structure degradation.[20–27]

APPJs have been applied to inactivate gram-positive and gram-negative bacteria due to the effective and rapid inactivation, non-toxic residues, and cost effectiveness. For example, Matthes et al. investigated the antimicrobial efficacy of the Ar/Ar+$O_2$ APPJ on *P. aeruginosa* and *S. epidermidis* biofilms *in vitro*. The inactivation effects were significant and depended on the gas mixture, bacteria strain, and exposure time.[28] Koban et al. evaluated the antifungal effects of an APPJ on *C. albicans*, *S. mutans*, and multiple-species human saliva biofilms *in vitro* and showed that the low-temperature plasma treatment was a promising alternative against biofilms to chemical antiseptics.[29,30] Gorynia et al. evaluated the antibacterial effects of Ar APPJ against *S. sanguinis* biofilms[31] and Xiong et al. discovered that the APPJ plasma could penetrate *P. gingivalis* biofilms to a thickness of 15 μm.[32] Pei et al. studied the inactivation effects of a room-temperature air plasma jet on *E. faecalis* biofilms and found the plasma jet penetrated the 25.5 μm thick biofilm all the way to the bottom.[33] However, apart from the antimicrobial efficacy, less attention has been paid to the detailed plasma-driven inactivation mechanisms against biofilms. *Staphylococcus aureus* (*S. aureus*), a gram-positive bacterium which is a common cause of skin infection, respiratory disease, and burned tissues infection, is capable of forming biofilms on human skins, biomedical devices such as catheters, and other biomaterials leading to chronic infections in patients.[34] In this work, a home-made helium APPJ is employed to treat biofilm and adherent *S. aureus* and the antimicrobial effects and related mechanisms are studied.

## 2. Plasma Source, Materials, and Methods

### 2.1. Atmospheric-Pressure Plasma Jet (APPJ)

The schematic of the APPJ system is shown in Figure 1. In the center of a quartz capillary (inner diameter of 2 mm, outer diameter of 4 mm, and total length of 80 mm), a copper rod (diameter of 2 mm and 100 mm long) was mounted with one side sealed as a single electrode and tightly wrapped in a PTFE shell. A small quartz tube (length of 20 mm, inner diameter of 4 mm, and outer diameter of 6 mm) was connected to the shell as a nozzle.[23] A sinusoidal AC high-voltage supply provided $V_{p\text{-}p}$ of 20 kV at a frequency of 38 kHz. Helium (99.995%) was the working gas and the typical flow rate was 6.7 standard liter per minute (SLM).

**Cultivation of *S. aureus* Bacterial Suspension**

The *S. aureus* strain NCTC 8325 with a strong biofilm-forming capacity was incubated in the tryptic soy broth (TSB) soybean-casein digestive medium (BD, Bacto, Franklin Lakes).[35] In each experiment, a freshly isolated single bacteria colony was picked from a TSB agar plate, transferred to 2 mL of the TSB medium, and incubated while agitated (225 rpm) at 37 °C overnight to a final concentration of approximately 1–2 × $10^9$ cells · $mL^{-1}$.

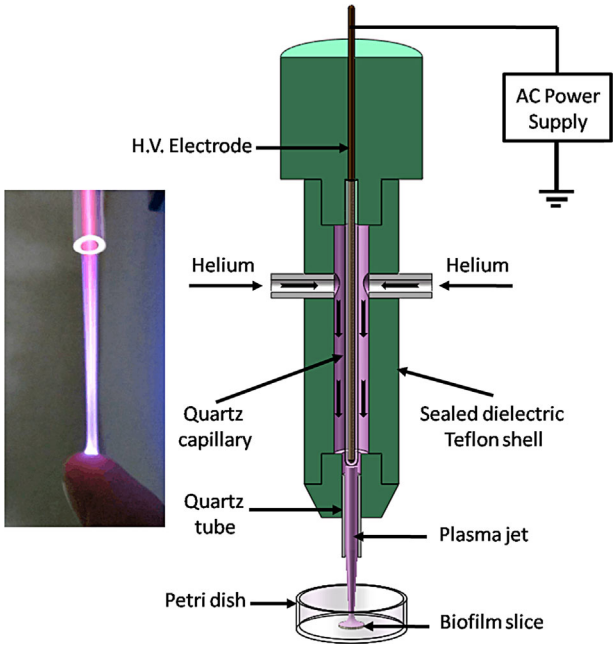


*Figure 1.* Schematic of the APPJ device and photograph of the helium APPJ.




DOI: 10.1002/ppap.201500006

**Formation of *S. aureus* Biofilms and Adherent *S. aureus***

To form the *S. aureus* biofilms, the overnight culture of *S. aureus* was diluted with the TSBG (TSB with 0.2% glucose) medium to $1–2 \times 10^7$ cells $\cdot$ mL$^{-1}$ and inoculated onto borosilicate slices (diameter of 6 mm and thickness of 0.2 mm, WHB Biology, Shanghai, China) placed in the wells of a 24-well flat bottom cell culture plate (polystyrene, Costar 3524, Corning Inc., Corning, NY; 1 slice/well, 2 mL medium/well). The plate was incubated at 37 °C for up to 12 h without medium change or agitation. Thereafter, the supernatants were removed and slices with the formed biofilms on their upper surface were taken out cautiously, transferred to sterile petri dishes (1 slice/petri dish), and washed with sterile physiological saline to remove the planktonic or loosely attached bacteria.[36] The biofilm slices were placed in an incubator at 37 °C for surface semi-dryness prior to plasma jet exposure.

To produce the adherent *S. aureus*, 10 μL of the overnight culture of planktonic *S. aureus* ($1–2 \times 10^9$ CFU $\cdot$ mL$^{-1}$) were dripped onto the same kind of borosilicate slices and placed in an incubator at 37 °C to evaporate the liquid to semi-dryness.

### 2.2. Plasma Exposure

The petri dish with the biofilm or adherent bacteria slice was positioned on a hand-controlled x/y/z table (Zolix, Beijing, China) below the nozzle of the plasma jet which was aimed at the center of the slice from a distance of 10 mm thus allowing exposure of the entire sample. The treatment time was varied from 0 to 10 min.

### 2.3. Optical Emission Spectroscopy (OES)

The optical emission spectra were recorded on the AvaSpec-2048-8-RM spectrometer equipped with gratings of 2 400 grooves $\cdot$ mm$^{-1}$ and an optical fiber located at a distance of 10 mm from the nozzle of the plasma jet.

### 2.4. Mass Spectrometry (MS)

A molecular-beam mass spectrometer (MBMS, Hiden EQP mass/energy analyzer HPR 60) was operated in the time-averaged mode. The distance between the exit of the plasma jet and orifice of the mass spectrometer was 10 mm.

### 2.5. Cultivability of Biofilm and Adherent *S. aureus*

The cultivable bacteria were assessed by counting colony-forming units (CFUs) on agar plates to evaluate the plasma treatment effects and calculate the D-value (time required to reduce 90% of the cultivable bacteria population). After plasma exposure, the biofilm or adherent *S. aureus* slices were taken out from the petri dish and placed in a 10 mL borosilicate glass culture tube (1 slice/tube), respectively. Each sample was resuspended (dispersed in an ultrasonic bath for 5 min and then vortexed) in 2 mL of sterile physiological saline (0.9% NaCl solution) and the proper decimal dilution was performed according to the bacterial concentration in the resuspension for easy counting. Afterwards, 100 μL of the diluted solution was spread on TSB agar plates in triplicates and incubated at 37 °C overnight to count the cultivable bacteria populations. The antimicrobial effects were determined according to the differences in the population of CFUs.

### 2.6. Membrane Integrity of Biofilm *S. aureus*

LIVE/DEAD staining, in combination with confocal laser-scanning microscopy (CLSM), was employed to observe the plasma treatment effects on *S. aureus* biofilms based on the bacterial membrane integrity. The LIVE/DEAD BacLight bacterial viability kit (L7012, Molecular Probes, Carlsbad) was prepared according to the manufacturer's instructions. It contained two nucleic acid dyes: SYTO 9 (exhibiting green fluorescence and often used to map living bacteria cells with intact membranes) and propidium iodide (PI with red fluorescence which can only transfuse through a damaged cell membrane and is often used to trace membrane-damaged dead bacteria). The biofilms were incubated on glass bottom microwell dishes (part no. P35G-1.5.20-C, MatTek Co., Ashland, MA). During exposure, the plasma jet was aimed at the center of the microwell. The treated/untreated biofilms were then washed with 1 mL of $dH_2O$ twice and 200 μL of the dye mixture was dripped onto the microwell to fully cover it. After incubation at room temperature in darkness for 15 min, each sample was rinsed again with 1 mL of $dH_2O$ twice to remove the dye residues. The samples were then examined by CLSM (Zeiss LSM710, Carl Zeiss, Jena, Germany). The image stacks along the *z*-axis were captured using the Zeiss ZEN 2010 software package (Carl Zeiss, Jena, Germany) by a Plan-Apochromat 20×/0.8 M27 objective lens with the excitation and emission wavelengths of 485/530 nm (for SYTO 9) and 485/630 nm (for PI). The interval in the *z*-axis was set at 1.237 μm.[32,33,37,38]

### 2.7. Intracellular Reactive Oxygen Species (ROS)

To detect the intra-bacterial ROS in the biofilm, the intracellular ROS monitoring probe 2,7-dichlorodihydro-fluorescein diacetate (DCFH-DA, Reactive Oxygen Species Assay Kit S0033, Beyotime, Shanghai, China) was utilized. DCFH-DA was a cell-permeable, non-fluorescent probe, which could be intracellularly de-esterified. DCFH could be

oxidized by intracellular ROS to highly fluorescent dichlorofluorescein (DCF) as the ROS indicator.[39] After plasma exposure, the biofilms formed on microwell dishes were rinsed with 1 mL of $dH_2O$ twice and 1 mL of DCFH-DA solution (10 μM) was added to fully cover the biofilms, followed by incubation at 37 °C for 20 min in darkness.[40,41] After incubation, the biofilms were cautiously rinsed with $dH_2O$ three times to remove the residual DCFH-DA that had not penetrated the cells. The *z*-axis image stacks and related fluorescence intensities of the DCF were captured and collected using CLSM with Zeiss ZEN 2010 software package by setting the excitation and emission wavelengths at 488 and 525 nm, respectively. The *z*-axis interval was 1.500 μm.

### 2.8. Statistical Analysis

All the experiments were repeated in three independent assays and three replicates each. The CFU countings were transformed to log 10 $mL^{-1}$. The mean values and standard deviations (SD) were derived from nine measurements and the error bars represent the standard deviation of the mean value. The *p* values in the Student's t-tests were calculated to determine the validity (significant level) of the surviving factors of *S. aureus* after the APPJ treatment.

## 3. Results and Discussion

### 3.1. Characteristics of the Helium APPJ

Optical emission spectroscopy (OES) is commonly used to determine plasma parameters such as the excited species. The typical optical emission intensity of this He plasma jet is in a range of 200–1050 nm (Figure 2) and excited OH (306–310 nm), various nitrogen species, He multi-emission lines, and atomic oxygen O (777.2 nm, 844 nm) are observed. According to previous studies,[42–44] reactive species such as O and OH play crucial roles in inactivating cells and causing cell lysis *via* oxidation of bacterial components. In prokaryotic cells, the electron transport chain which supports most cellular bio-physical/chemical reactions is located in the cell membrane.[45] These reactive species can impact the lipid membranes from the exterior to cause functional perturbation of the cell membranes, thereby leading to various intra-bacterial biological effects and consequent structural damage due to lipid peroxidation.[46]

The He APPJs are very mild and can be touched with no harm (Figure 1).[18] As *S. aureus* is very sensitive to a high temperature, the low-temperature operation excludes the effects of thermal bacteria deactivation and the more likely mechamism stems from plasma-generated reactive radicals and charged particles. Figure 3a and b depict the mass spectra acquired at a distance of 10 mm from the exit of the plasma jet in the time-averaged mode. Ions up to 100 amu are detected. The positive mass spectrum in Figure 3a shows about 20 species created in the He plasma jet-air interaction with the predominant speceis being $N_2^+$, $O_2^+$, $NO^+$, $H_2O^+$, $H_3O^+$,$H_3O^+(H_2O)$, and $N_2H^+$ together with small amounts of $N^+$, $O^+$, $OH^+$, and $H_3O^+(H_2O)_2$. The negative mass spectrum reveals about 30 species with the main species

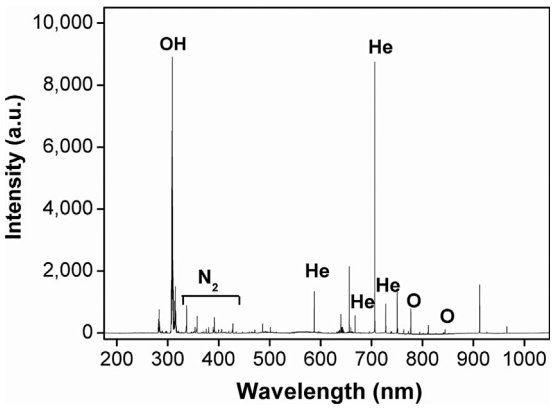


*Figure 2.* Optical emission spectrum in the range of 200–1050 nm acquired at a distance of 10 mm below the nozzle of the plasma jet.

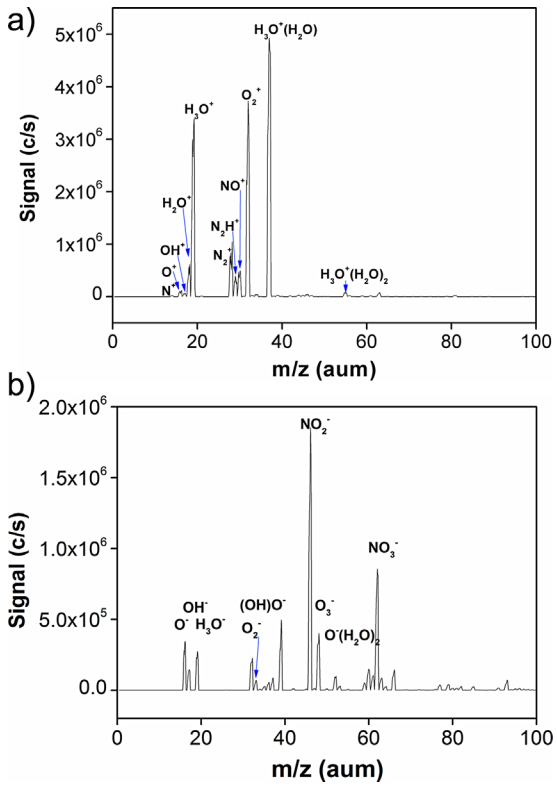


*Figure 3.* (a) Positive mass spectra and (b) Negative mass spectra acquried from the plasma at a distance of 10 mm from the nozzle.



DOI: 10.1002/ppap.201500006

being $O^-$, $O_2^-$, $O_3^-$, $OH^-$, $(OH)O^-$, $H_3O^-$, $NO_2^-$, and $NO_3^-$ (Figure 3b). In general, microbial biofilms contain more than 90% water and there are water channels in the biofilm structure. $H_2O$ molecules are adherent to the biofilm surface due to surface tension (semi-dryness).[1,2] The adherent bacteria also have $H_2O$ molecules on the surface and in the intercellular space (semi-dryness). The effect of ions impinging on the biofilm and adherent *S. aureus* is expected to be expressed in induced liquid chemistry potentially producing radicals such as OH or increasing the acidity of the surrounding environment, thereby causing oxidative damage detrimental to cell survival.[44,46,47]

### 3.2. Survival Curves of Biofilm and Adherent *S. aureus*

Figure 4 exhibits the survival curves of the biofilm and adherent *S. aureus* after plasma exposure between 0 and 10 min obtained by CFU counting. They indicate statistically significant antimicrobial effects on the biofilms and adherent cells compared to the untreated samples. The biofilms are obviously more resistant to the plasma treatment than adherent bacteria. The total bacteria population before the treatment is about $6.59 \pm 0.61$ log10 CFU $\cdot$ mL$^{-1}$ in the biofilms and $7.22 \pm 0.27$ log10 CFU $\cdot$ mL$^{-1}$ for the adherent cells. The D-value calculated from the biofilms (about 52 s) is larger than that from the adherent bacteria (about 29 s). Hence, the 10 min APPJ treatment is effective leading to a reduction of 3.06 log10 CFU $\cdot$ mL$^{-1}$ (more than 99.9%) for the biofilm and 7.22 log10 CFU $\cdot$ mL$^{-1}$ (complete inactivation) for the adherent *S. aureus*. In this study, the biofilms and adherent cells without plasma treatment are used as control samples to demonstrate the susceptibility to the helium APPJ.

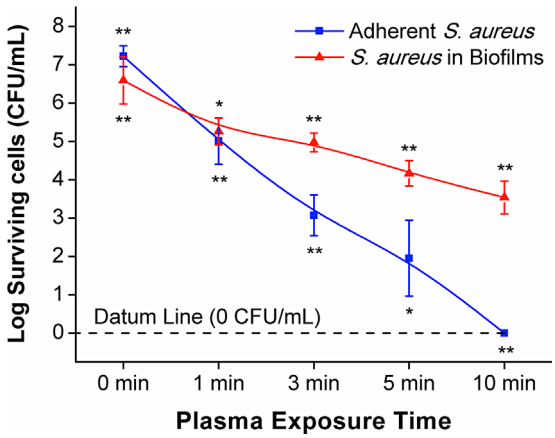


*Figure 4.* Log survival curves of the helium APPJ treated *S. aureus* biofilms and adherent *S. aureus*. Each point represents the mean of nine values $\pm$ SD (standard deviation). The black dash line represents the numerical value "o" (o CFU $\cdot$ mL$^{-1}$) as the datum line. The asterisks (*) above the two curves are for uptriangle (▲) data points, and asterisks below the two curves are for square (■) data points; significant level: $^*p < 0.05$; $^{**}p < 0.01$.

In comparison to recently published reports on the efficacy of APPJ treatment on microbial biofilms, the antibacterial effects observed from our experiments are good and consistent. For instance, Alkawareek et al. investigated the inactivation effects of a $He/O_2$ cold APPJ on *P. aeruginosa* biofilms *in vitro* and a more than 4-log (99.99%) CFU/peg reduction was achieved within 4 min of exposure at 20 kHz. While operating frequency at 40 kHz, complete eradication was observed after 4 min of plasma exposure.[48] In this study, the total reduction for *S. aureus* biofilms after APPJ exposure for 10 min is 3.06 log (99.9%) CFU $\cdot$ cm$^{-3}$. The admixture of oxygen may lead to more ROS in the plasma flow causing the difference in the antimicrobial efficacy. The different bacterial strains used may be another possible reason. Matthes et al. utilized the APPJ source to inactivate *P. aeruginosa* and *S. epidermidis* biofilms *in vitro* and considerable antimicrobial effects were observed. A 5 min Ar APPJ treatment led to a total reduction of 5.41-log CFU cm$^{-2}$ bacteria for *P. aeruginosa* biofilms and 3.14-log CFU $\cdot$ cm$^{-2}$ bacteria for *S. epidermidis* biofilms. In our study, 2.43-log CFU $\cdot$ cm$^{-3}$ bacteria reduction is observed from the *S. aureus* biofilms after the same treatment time. The effectiveness may depend on the working gas, bacterial strain, and plasma dose.[28] Abramzon et al. investigated the antifungal capacity of a $He/N_2$ RF (13.56 MHz) APPJ on *C. violaceum* biofilms and found that 10 min plasma exposure led to a more than 2-log CFU $\cdot$ cm$^{-3}$ reduction in the biofilm bacteria with a D-value of about 2.3 min.[49] In comparison, the antibacterial efficacy of our present He APPJ treatment on *S. aureus* biofilms is better albeit not significantly. Matthes et al. also investigated the treatment effect of 6 repeated application steps of Ar plasma (kinpen09) on *S. aureus* biofilms. The antimicrobial effect was stable and repeated application of the APPJ was found to be a promising choice to cure *S. aureus* biofilm-associated infected wounds without development of plasma resistance.[50]

In order to inactivate bacteria below the surface layer, the plasma discharge-driven reactive species have to penetrate the biofilm layer-by-layer, but there is no such stable and sophisticated structure for the adherent cells. Furthermore, as the extracellular polymeric substances (EPS) which encase these bacteria are mainly composed of proteins and polysaccharides, these organic substances act as a barrier to protect cells from physical and chemical stress. The plasma encounters the EPS first and then impacts the bacteria located in the biofilms compared to direct attack on adherent cells. Therefore, without protection rendered by the EPS and complex matrix structure, adherent bacteria are more rapidly damaged and killed. The inactivation processes

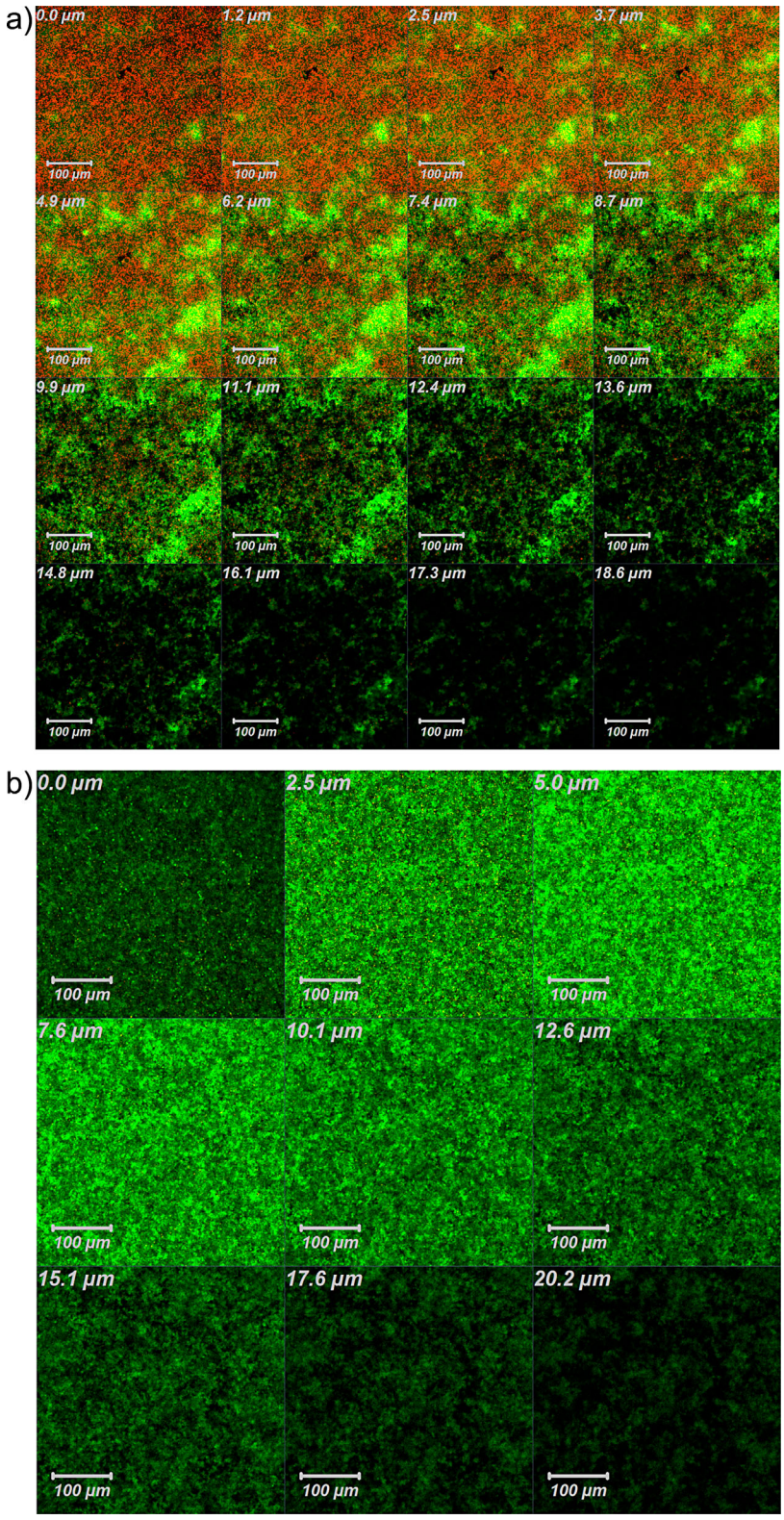


*Figure 5.* (a) Z-stack CLSM images of the bacterial membrane integrity detection probe SYTO 9/PI stained, 5 min helium APPJ treated *S. aureus* biofilm and (b) Z-stack CLSM images of the bacterial membrane integrity detection probe SYTO 9/PI stained, plasma-untreated *S. aureus* biofilm (serving as control).

and mechanisms of biofilms are more complicated than those of adherent bacteria upon plasma attack.

### 3.3. Membrane Integrity of Biofilm *S. aureus*

The *z*-axis CLSM image stacks acquired from the SYTO 9/PI stained 5 min plasma-treated *S. aureus* biofilms are displayed in Figure 5a. The top layers (1st to 4th) are predominantly red, implying that large amounts of bacteria in these layers have damaged membranes. With increasing depths, red dots diminish gradually until they are rarely spotted, whereas the proportion of green ones increases, signifying that lots of bacteria in the layers underneath still have intact cellular membranes. Figure 5b serves as the untreated control.

### 3.4. Intracellular ROS of Biofilm *S. aureus*

The intracellular ROS is monitored to investigate its role in the bacteria deactivation process and the results are presented in Figures 6 and 7. Figure 6a displays the Z-stack images of ROS concentrations in the biofilm after plasma exposure for 5 min. The fluorescence intensities of DCF (at 488/525 nm, indicating intracellular ROS) in the 1st to 3rd layers of *S. aureus* biofilms decrease whereas those observed from the layers beneath rise compared to the control sample (untreated, dark green due to the intracellular ROS produced by their natural and well-balanced bacterial aerobic metabolism) in Figure 6b. As shown in Figure 5a, a large number of *S. aureus* in the top layers has damaged membrane after plasma treatment for 5 min, implying that highly fluorescent DCF cannot be fully encased by the damaged bacterial membrane but leaks out and is washed away. Moreover, the main site for bacterial aerobic metabolism is through the cell membrane by functions of a series of membrane proteins (enzymes) and the breakage of cellular membranes suggests that the intracellular pathways of ROS

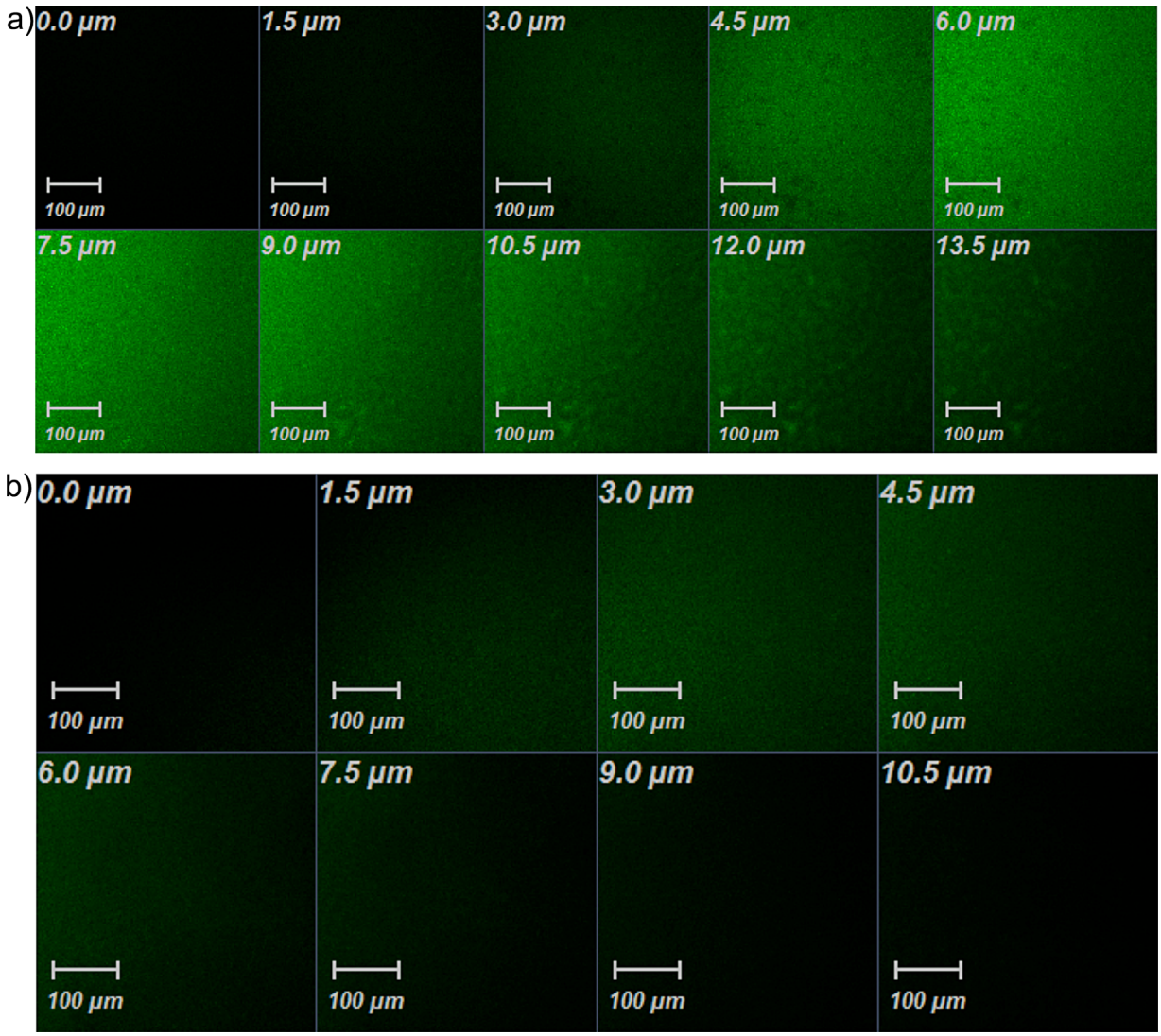


*Figure 6.* (a) Z-stack CLSM images of the intracellular ROS fluorescent probe DCFH-DA stained, 5 min helium APPJ treated *S. aureus* biofilm and (b) Z-stack CLSM images of the intracellular ROS fluorescent probe DCFH-DA stained, plasma-untreated *S. aureus* biofilm (serving as control).

generation are interrupted. This may explain why bacteria in the top three layers (0–4.5 μm) in the *S. aureus* biofilm show lower DCF fluorescence intensity (detected intracellular ROS concentrations) than the untreated sample.

However, large amounts of biofilm *S. aureus* located in layers beneath have intact membranes (shown in Figure 5a) and exhibit enhancing DCF fluorescence intensity. The electron transport chain of *S. aureus* is located in the cell membrane which is the major site of successive single-electron reduction to oxygen, producing intracellularly generated ROS of $O_2^-$, $H_2O_2$, as well as highly toxic and indiscriminately reactive OH.[45] According to Figure 2 and 3, the APPJ used in this study generates various reactive species such as O, $O_2^-$, OH, etc.. Therefore, the plasma discharge, especially plasma-generated reactive species, may induce the intracellular production of ROS in these bacteria. In general, reactive plasma species such as excited atoms, molecules, and radicals are considered to directly impinge on the micro-organisms from the exterior (targeting at the extracellular matrix and cellular outer membrane, etc.) as oxidants, resulting in acute oxidative processes on the bacterial structure including breaking chemical bonds, producing volatile compounds and molecular fragments, and finally leading to biocidal effects.[21–23,51–56] The accumulated intracellular ROS may also perturb the cellular functions and damage the cellular structure from the interior of the bacteria,[57] thus synergistically resulting in bacteria inactivation in combination with direct plasma etching of the bacteria from the exterior. Specifically, the 4th to 9th layers exhibit the best

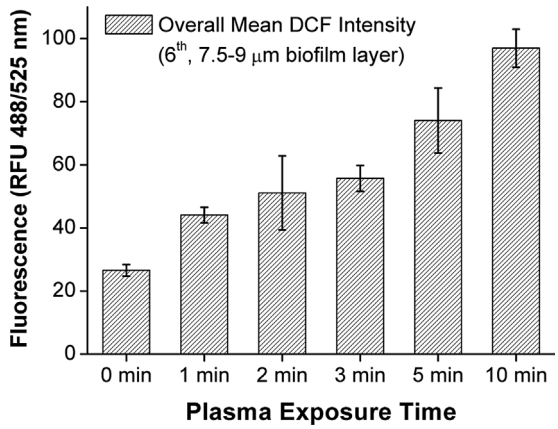


*Figure 7.* Overall mean DCF fluorescence intensities (RFU, at 488/525 nm) of the 6th layer (7.5–9 μm) in the plasma-treated biofilm, with the highly fluorescent DCF being an indicator of intracellular ROS.

ROS accumulation effects possibly due to the plasma exposure dose and restricted plasma treating effects on the biofilms, showing an impact depth of ROS accumulation of approximately 12.0 μm.

Figure 7 exhibits the overall mean DCF fluorescence intensity (at 488/525 nm) of *S. aureus* in the 6th layer of biofilm (7.5–9 μm) after plasma exposure for different periods of time. The gradual rise in the DCF intensity suggests accumulation of intracellular ROS in this layer and a relatively high value of 97 RFU (relative fluorescence units) is detected after treatment for 10 min. Thus, increasing the plasma dose may stimulate and enhance endogenous production of ROS for bacteria located in the same position of the biofilms. Therefore, the incremental intracellular ROS results in oxidative damage pernicious to cell survival when a certain threshold of the cellular oxidative stress response to counteract the plasma-driven intra-bacterial oxidation potential is exceeded.

## 4. Conclusion

The antimicrobial effects and mechanism of a helium APPJ on biofilm and adherent *S. aureus* are investigated. The D-value obtained by counting CFUs is 52 s with a total reduction of 3.06 log10 CFU · $mL^{-1}$ (more than 99.9%) after plasma exposure for 10 min, whereas that of adherent *S. aureus* is only 29 s showing a total reduction of 7.22 log10 CFU · $mL^{-1}$ (complete inactivation). Therefore, *S. aureus* biofilms are more resistant to the plasma than adherent ones. The shading effects provided by the biofilm EPS, matrix structure, and surface bacteria may explain the phenomenon. After plasma exposure for 5 min, *S. aureus* located in the top three layers (0–4.5 μm) of the biofilm possess lower intracellular ROS concentrations than the untreated sample, because the membranes of many bacteria in these layers are damaged. However, for bacteria in the layers underneath, the intracellular ROS intensities rise considerably. In particular, the 4th to 9th layers exhibit the best ROS accumulation effects and the ROS accumulation-dependent impact depth is about 12.0 μm after plasma exposure for 5 min. With respect to *S. aureus* in the 6th layer (7.5–9 μm), the intra-bacterial ROS intensities increase gradually and steadily with plasma dose. The plasma treatment induces intracellular production of ROS and plays pivotal and synergistic roles in the inactivation of microbial biofilms in conjunction with the direct etching effect.

Acknowledgements: This work was financially supported by the National Natural Science Foundation of China under grant nos. 11035005, 11475174, 11005126, and 11205203, Hefei Institutes of Physical Science, Chinese Academy of Sciences (CASHIPS) Dean funds no. YZJJ201331, City University of Hong Kong Strategic Research grant (SRG) no. 7004188, as well as Hong Kong Research Grants Council (RGC) General Research Funds (GRF) no. CityU 112212.

Received: January 9, 2015; Revised: March 16, 2015; Accepted: March 18, 2015;DOI: 10.1002/ppap.201500006

Keywords: microbial biofilm; non-thermal plasma; plasma jet; reactive oxygen species; sterilization/decontamination

[1] H.-C. Flemming, U. Szewzyk, T. Griebe, *"Biofilms: Investigative Methods & Applications"*, Technomic Pub. Co., Lancaster, PA. **2000**.
[2] H.-C. Flemming, A. Leis, International Water Association, "Extracellular polymeric substances: the construction materials of biofilms": selected proceedings of the 1st IWA International Conference on Microbial Extracellular Polymeric Substances, held in Mulheim, Germany, 2000, London: IWA, 2001.
[3] D. L. Bayliss, J. L. Walsh, F. Iza, G. Shama, J. Holah, M. G. Kong, *Plasma Process. Polym.* **2012**, *9*, 597.
[4] T. Bjarnsholt, *"Biofilm Infections"*, Springer, New York **2011**.
[5] S. G. Joshi, M. Paff, G. Friedman, G. Fridman, A. Fridman, A. D. Brooks, *Am. J. Infect. Control* **2010**, *38*, 293.
[6] Th. Von Woedtke, S. Reuter, K. Masur, K.-D. Weltmann, *Phys. Rep.* **2013**, *530*, 291.
[7] A. A. Fridman, G. Friedman, *"Plasma Medicine"*, Wiley, Chichester **2013**.
[8] G. Fridman, G. Friedman, A. Gutsol, A. B. Shekhter, V. N. Vasilets, A. Fridman, *Plasma Process. Polym.* **2008**, *5*, 503.
[9] M. G. Kong, G. Kroesen, G. Morfill, T. Nosenko, T. Shimizu, J. van Dijk, J. L. Zimmermann, *New J. Phys.* **2009**, *11*, 115012.
[10] M. Laroussi, C. Tendero, X. Lu, S. Alla, W. L. Hynes, *Plasma Process. Polym.* **2006**, *3*, 470.
[11] R. Burlica, R. G. Grim, K. Y. Shih, D. Balkwill, B. R. Locke, *Plasma Process. Polym.* **2010**, *7*, 640.

[12] G. Fridman, A. D. Brooks, M. Balasubramanian, A. Fridman, A. Gutsol, V. N. Vasilets, H. Ayan, G. Friedman, *Plasma Process. Polym.* **2007**, *4*, 370.
[13] M. Laroussi, *IEEE Trans. Plasma Sci.* **2009**, *37*, 714.
[14] C. Cheng, P. Liu, L. Xu, L. Y. Zhang, R. J. Zhan, W. R. Zhang, *Chin. Phys.* **2006**, *15*, 1544.
[15] C. Cheng, J. Shen, D. Z. Xiao, H. B. Xie, Y. Lan, S. D. Fang, Y. D. Meng, K. C. Paul, *Chin. Phys. B* **2014**, *23*, 7.
[16] X. Lu, Z. Jiang, Q. Xiong, Z. Tang, X. Hu, Y. Pan, *Appl. Phys. Lett.* **2008**, *92*, 081502.
[17] X. Lu, Z. Jiang, Q. Xiong, Z. Tang, Y. Pan, *Appl. Phys. Lett.* **2008**, *92*, 151504.
[18] X. Lu, G. V. Naidis, M. Laroussi, K. Ostrikov, *Phys. Rep.* **2014**, *540*, 123.
[19] C. Zhang, T. Shao, Y. Zhou, Z. Fang, P. Yan, W. Yang, *Appl. Phys. Lett.* **2014**, *105*, 044102.
[20] S. Ikawa, K. Kitano, S. Hamaguchi, *Plasma Process. Polym.* **2010**, *7*, 33.
[21] P. Lukes, E. Dolezalova, I. Sisrova, M. Clupek, *Plasma Sources Sci. Technol.* **2014**, *23*, 015019.
[22] K. P. Arjunan, A. M. Clyne, *Plasma Process. Polym.* **2011**, *8*, 1154.
[23] J. Shen, C. Cheng, S. D. Fang, H. B. Xie, Y. Lan, G. H. Ni, Y. D. Meng, J. R. Luo, X. K. Wang, *Appl. Phys. Express* **2012**, *5*, 036201.
[24] H. Yasuda, T. Miura, H. Kurita, K. Takashima, A. Mizuno, *Plasma Process. Polym.* **2010**, *7*, 301.
[25] B. Gweon, D. Kim, D. B. Kim, H. Jung, W. Choe, J. H. Shin, *Appl. Phys. Lett.* **2010**, *96*, 101501.
[26] J. Choi, A.-A. H. Mohamed, S. K. Kang, K. C. Woo, K. T. Kim, J. K. Lee, *Plasma Process. Polym.* **2010**, *7*, 258.
[27] M. Laroussi, T. Akan, *Plasma Process. Polym.* **2007**, *4*, 777.
[28] R. Matthes, I. Koban, C. Bender, K. Masur, E. Kindel, K.-D. Weltmann, T. Kocher, A. Kramer, N.-O. Hübner, *Plasma Process. Polym.* **2013**, *10*, 161.
[29] I. Koban, R. Matthes, N.-O. Hübner, A. Welk, P. Meisel, B. Holtfreter, R. Sietmann, E. Kindel, K.-D. Weltmann, A. Kramer, T. Kocher, *New J. Phys.* **2010**, *12*, 073039.
[30] I. Koban, B. Holtfreter, N.-O. Hübner, R. Matthes, R. Sietmann, E. Kindel, K.-D. Weltmann, A. Welk, A. Kramer, T. Kocher, *J. Clin. Periodontol.* **2011**, *38*, 956.
[31] S. Gorynia, I. Koban, R. Matthes, A. Welk, S. Gorynia, N.-O. Hübner, T. Kocher, A. Kramer, *GMS Hyg. Infect. Control* **2013**, *8*, Doc01.
[32] Z. Xiong, T. Du, X. Lu, Y. Cao, Y. Pan, *Appl. Phys. Lett.* **2011**, *98*, 221503.
[33] X. Pei, X. Lu, J. Liu, D. Liu, Y. Yang, K. Ostrikov, P. K. Chu, Y. Pan, *J. Phys. D Appl. Phys.* **2012**, *45*, 165205.
[34] A. L. Goodman, *J. Bacteriol.* **2010**, *192*, 5273.
[35] D. Yu, L. Zhao, T. Xue, B. Sun, *BMC Microbiol.* **2012**, *12*, 288.
[36] L. Zhao, T. Xue, F. Shang, H. Sun, B. Sun, *Infect. Immun.* **2010**, *78*, 3506.
[37] Y. B. You, T. Xue, L. Y. Cao, L. P. Zhao, H. P. Sun, B. L. Sim, *Int. J. Med. Microbiol.* **2014**, *304*, 603.
[38] S. Rupf, A. N. Idlibi, F. Al Marrawi, M. Hannig, A. Schubert, L. von Mueller, W. Spitzer, H. Holtmann, A. Lehmann, A. Rueppell, A. Schindler, *PLoS ONE* **2011**, *6*, e25893.
[39] B. Kalyanaraman, V. Darley-Usmar, K. J. A. Davies, P. A. Dennery, H. J. Forman, M. B. Grisham, G. E. Mann, K. Moore, L. J. Roberts Ii, H. Ischiropoulos, *Free Radical Bio. Med.* **2012**, *52*, 1.
[40] H.-L. Su, C.-C. Chou, D.-J. Hung, S.-H. Lin, I. Pao, J.-H. Lin, F.-L. Huang, R.-X. Dong, J.-J. Lin, *Biomaterials* **2009**, *30*, 5979.
[41] A. L. Santos, N. Gomes, I. Henriques, A. Almeida, A. Correia, Â. Cunha, *J. Photoch. Photobio. B* **2012**, *117*, 40.
[42] X. Lu, T. Ye, Y. Cao, Z. Sun, Q. Xiong, Z. Tang, Z. Xiong, J. Hu, Z. Jiang, Y. Pan, *J. Appl. Phys.* **2008**, *104*, 053309.
[43] D. X. Liu, M. Z. Rong, X. H. Wang, F. Iza, M. G. Kong, P. Bruggeman, *Plasma Process. Polym.* **2010**, *7*, 846.
[44] D. B. Graves, *J. Phys. D Appl. Phys.* **2012**, *45*, 263001.
[45] K. Gerald, *"Cell and Molecular Biology: Concepts and Experiments"*, Wiley and Sons, Hoboken **2005**.
[46] X. Yan, Z. Xiong, F. Zou, S. Zhao, X. Lu, G. Yang, G. He, K. K. Ostrikov, *Plasma Process. Polym.* **2012**, *9*, 59.
[47] C. A. J. Van Gils, S. Hofmann, B. Boekema, R. Brandenburg, P. J. Bruggeman, *J. Phys. D Appl. Phys.* **2013**, *46*, 175203.
[48] M. Y. Alkawareek, Q. T. Algwari, S. P. Gorman, W. G. Graham, D. O'Connell, B. F. Gilmore, *FEMS Immunol. Med. Microbiol.* **2012**, *65*, 381.
[49] N. Abramzon, J. C. Joaquin, J. Bray, G. Brelles-Marino, *IEEE Trans. Plasma Sci.* **2006**, *34*, 1304.
[50] R. Matthes, O. Assadian, A. Kramer, *GMS Hyg. Infect. Control* **2014**, *9*, Doc17.
[51] K. Fricke, I. Koban, H. Tresp, L. Jablonowski, K. Schroeder, A. Kramer, K.-D. Weltmann, T. von Woedtke, T. Kocher, *PLoS ONE* **2012**, *7*, e42539.
[52] F. Marchal, H. Robert, N. Merbahi, C. Fontagné-Faucher, M. Yousfi, C. E. Romain, O. Eichwald, C. Rondel, B. Gabriel, *J. Phys. D Appl. Phys.* **2012**, *45*, 345202.
[53] J. C. Joaquin, C. Kwan, N. Abramzon, K. Vandervoort, G. Brelles-Marino, *Microbiology* **2009**, *155*, 724.
[54] R. Pompl, F. Jamitzky, T. Shimizu, B. Steffes, W. Bunk, H.-U. Schmidt, M. Georgi, K. Ramrath, W. Stolz, R. W. Stark, *New J. Phys.* **2009**, *11*, 115023.
[55] F. Rossi, O. Kylián, M. Hasiwa, *Plasma Process. Polym.* **2006**, *3*, 431.
[56] S. Rupf, A. Lehmann, M. Hannig, B. Schäfer, A. Schubert, U. Feldmann, A. Schindler, *J. Med. Microbiol.* **2010**, *59*, 206.
[57] R. A. Miller, B. E. Britigan, *Clin. Microbiol. Rev.* **1997**, *10*, 1.